EUROPEAN ORGANIZATION FOR NUCLEAR RESEARCH

CERN-EP/89-132
October 13th,1989

Determination of the Number of Light Neutrino Species

12 October 1989

The ALEPH Collaboration

D. Decamp, B. Deschizeaux, J.-P. Lees, M.-N. Minard

Laboratoire de Physique des Particules (LAPP), 74019 Annecy-le-Vieux Cedex, France

J.M. Crespo, M. Delfino, E. Fernandez[1], M. Martinez, R. Miquel, M.L. Mir, S. Orteu, A. Pacheco, J.A. Perlas, E. Tubau

Laboratorio de Fisica de Altas Energias, Universidad Autonoma de Barcelona, 08193 Bellaterra (Barcelona), Spain[9]

M.G. Catanesi, M. De Palma, A. Farilla, G. Iaselli, G. Maggi, A. Mastrogiacomo, S. Natali, S. Nuzzo, A. Ranieri, G. Raso, F. Romano, F. Ruggieri, G. Selvaggi, L. Silvestris, P. Tempesta, G. Zito

INFN Sezione di Bari e Dipartimento di Fisica dell' Università, 70126 Bari, Italy

Y. Chen, D. Huang, J. Lin, T. Ruan, T. Wang, W. Wu, Y. Xie, D. Xu, R. Xu, J. Zhang, W. Zhao

Institute of High-Energy Physics, Academia Sinica, Beijing, The People's Republic of China

H. Albrecht[3], F. Bird, E. Blucher, T. Charity, H. Drevermann, Ll. Garrido, C. Grab, R. Hagelberg, S. Haywood, B. Jost, M. Kasemann, G. Kellner, J. Knobloch, A. Lacourt, I. Lehraus, T. Lohse, D. Lüke[3], A. Marchioro, P. Mato, J. May, V. Mertens, A. Minten, A. Miotto, P. Palazzi, M. Pepe-Altarelli, F. Ranjard, J. Richstein[4], A. Roth, J. Rothberg[5], H. Rotscheidt, W. von Rüden, D. Schlatter, R. St.Denis, M. Takashima, M. Talby, H. Taureg, W. Tejessy, H. Wachsmuth, S. Wheeler, W. Wiedenmann, W. Witzeling, J. Wotschack

European Organization for Nuclear Research (CERN), 1211 Geneva 23, Switzerland

Z. Ajaltouni, M. Bardadin-Otwinowska, A. Falvard, P. Gay, P. Henrard, J. Jousset, B. Michel, J-C. Montret, D. Pallin, P. Perret, J. Prat, J. Proriol, F. Prulhière

Laboratoire de Physique Corpusculaire, Université Blaise Pascal, Clermont-Ferrand, 63177 Aubiere, France

(Submitted to Physics Letters B)

H. Bertelsen, F. Hansen, J.R. Hansen, J.D. Hansen, P.H. Hansen, A. Lindahl, B. Madsen, R. Møllerud, B.S. Nilsson, G. Petersen

Niels Bohr Institute, 2100 Copenhagen, Danmark[10]

E. Simopoulou, A. Vayaki

Nuclear Research Center Demokritos (NRCD), Athens, Greece

J. Badier, D. Bernard, A. Blondel, G. Bonneaud, J. Bourotte, F. Braems, J.C. Brient, M.A. Ciocci, G. Fouque, R. Guirlet, P. Miné, A. Rougé, M. Rumpf, H. Videau, I. Videau[1], D. Zwierski

Laboratoire de Physique Nucléaire Hautes Energies, École Polytechnique, 91128 Palaiseau Cedex, France

D.J. Candlin

Department of Physics, University of Edinburgh, Edinburgh EH9 3JZ, United Kingdom[11]

A. Conti, G. Parrini

Dipartimento di Fisica, Università di Firenze, 50125 Firenze, Italy

M. Corden, C. Georgiopoulos, J.H. Goldman, M. Ikeda, D. Levinthal[16], J. Lannutti, M. Mermikides, L. Sawyer

High-Energy Particle Physics Laboratory, Florida State University, Tallahassee FL 32306, USA[13 14 15]

A. Antonelli, R. Baldini, G. Bencivenni, G. Bologna, F. Bossi, P. Campana, G. Capon, V. Chiarella, G. De Ninno, B. D'Ettorre-Piazzoli, G. Felici, P. Laurelli, G. Mannocchi, F. Murtas, G.P. Murtas, G. Nicoletti, P. Picchi, P. Zografou

Laboratori Nazionali dell'INFN (LNF-INFN), 00044 Frascati, Italy

B. Altoon, O. Boyle, A.J. Flavell, A.W. Halley, I. ten Have, J.A. Hearns, I.S. Hughes, J.G. Lynch, D.J. Martin, R. O'Neill, C. Raine, J.M. Scarr, K. Smith[1], A.S. Thompson

Department of Natural Philosophy, University of Glasgow, Glasgow G12 8QQ, United Kingdom[11]

B. Brandl, O. Braun, R. Geiges, C. Geweniger[1], P. Hanke, V. Hepp, E.E. Kluge, Y. Maumary, M. Panter, A. Putzer, B. Rensch, A. Stahl, K. Tittel, M. Wunsch

Institut für Hochenergiephysik, Universität Heidelberg, 6900 Heidelberg, Fed. Rep. of Germany[17]

G.J. Barber, A.T. Belk, R. Beuselinck, D.M. Binnie, W. Cameron[1], M. Cattaneo, P.J. Dornan, S. Dugeay, R.W. Forty, D.N. Gentry, J.F. Hassard, D.G. Miller, D.R. Price, J.K. Sedgbeer, I.R. Tomalin, G. Taylor

Department of Physics, Imperial College, London SW7 2BZ, United Kingdom[11]

P. Girtler, D. Kuhn, G. Rudolph

Institut für Experimentalphysik, Universität Innsbruck, 6020 Innsbruck, Austria

T.J. Brodbeck, C. Bowdery[1], A.J. Finch, F. Foster, G. Hughes, N.R. Keemer, M. Nuttall, B.S. Rowlingson, T. Sloan, S.W. Snow

Department of Physics, University of Lancaster, Lancaster LA1 4YB, United Kingdom[11]

T. Barczewski, L.A.T. Bauerdick, K. Kleinknecht[1], D. Pollmann[2], B. Renk, S. Roehn, H.-G. Sander, M. Schmelling, F. Steeg

Institut für Physik, Universität Mainz, 6500 Mainz, Fed. Rep. of Germany [17]

J-P. Albanese, J-J. Aubert, C. Benchouk, A. Bonissent, F. Etienne, R. Nacasch, P. Payre, B. Pietrzyk[1], Z. Qian

Centre de Physique des Particules, Faculté des Sciences de Luminy, 13288 Marseille, France

W. Blum, P. Cattaneo, M. Comin, B. Dehning, G. Cowan, H. Dietl, M. Fernandez-Bosman, D. Hauff, A. Jahn, E. Lange, G. Lütjens, G. Lutz, W. Männer, H-G. Moser, Y. Pan, R. Richter, A. Schwarz, R. Settles, U. Stiegler, U. Stierlin, G. Stimpfl[6], J. Thomas, G. Waltermann

Max-Planck-Institut für Physik und Astrophysik, Werner-Heisenberg-Institut für Physik, 8000 München, Fed. Rep. of Germany[17]

J. Boucrot, O. Callot, A. Cordier, M. Davier, G. de Bouard, G. Ganis, J.-F. Grivaz, Ph. Heusse, P. Janot, V. Journé, D.W. Kim, J. Lefrançois, D. Lloyd-Owen, A.-M. Lutz, P. Marotte, J.-J. Veillet

Laboratoire de l'Accéléateur Linéaire, Université de Paris-Sud, 91405 Orsay Cedex, France

S.R. Amendolia, G. Bagliesi, G. Batignani, L. Bosisio, U. Bottigli, C. Bradaschia, I. Ferrante, F. Fidecaro, L. Foà[1], E. Focardi, F. Forti, A. Giassi, M.A. Giorgi, F. Ligabue, A. Lusiani, E.B. Mannelli, P.S. Marrocchesi, A. Messineo, F. Palla, G. Sanguinetti, S. Scapellato, J. Steinberger, R. Tenchini, G. Tonelli, G. Triggiani

Dipartimento di Fisica dell'Università, INFN Sezione di Pisa, e Scuola Normale Superiore,56010 Pisa, Italy

J.M. Carter, M.G. Green, A.K. McKemey, P.V. March, T. Medcalf, M.R. Saich, J. Strong[1], R.M. Thomas, T. Wildish

Department of Physics, Royal Holloway & Bedford New College, University of London, Surrey TW20 OEX, United Kingdom[11]

D.R. Botterill, R.W. Clifft, T.R. Edgecock, M. Edwards, S.M. Fisher, D.L. Hill, T.J. Jones, G. McPherson, M. Morrissey, P.R. Norton, D.P. Salmon, G.J. Tappern, J.C. Thompson, J. Harvey

High-Energy Physics Division, Rutherford Appleton Laboratory, Chilton, Didcot, OXON OX11 OQX, United Kingdom[11]

B. Bloch-Devaux, P. Colas, C. Klopfenstein, E. Lançon, E. Locci, S. Loucatos, L. Mirabito, E. Monnier, P. Perez, F. Perrier, B. Pignard, J. Rander, J.-F. Renardy, A. Roussarie, J.-P. Schuller, R. Turlay

Département de Physique des Particules Élémentaires, CEN-Saclay, 91191 Gif-sur-Yvette Cedex, France

J.G. Ashman, C.N. Booth, F. Combley, M. Dinsdale, J. Martin, D. Parker, L.F. Thompson

Department of Physics, University of Sheffield, Sheffield S3 7RH, United Kingdom[11]

S. Brandt, H. Burkhardt, C. Grupen, H. Meinhard, E. Neugebauer, U. Schäfer, H. Seywerd, K. Stupperich

Fachbereich Physik, Universität Siegen, 5900 Siegen, Fed. Rep. of Germany[17]

B. Gobbo, F. Liello, E. Milotti, F. Ragusa[7], L. Rolandi[1]

Dipartimento di Fisica, Università di Trieste e INFN Sezione di Trieste, 34127 Trieste, Italy

L. Bellantoni, J.F. Boudreau, D. Cinabro, J.S. Conway, D.F. Cowen, Z. Feng, J.L. Harton, J. Hilgart, R.C. Jared[8], R.P. Johnson, B.W. LeClaire, Y.B. Pan, T. Parker, J.R. Pater, Y. Saadi, V. Sharma, J.A. Wear, F.V. Weber, Sau Lan Wu, S.T. Xue, G. Zobernig

Department of Physics, University of Wisconsin, Madison, Wisconsin 53706, USA [12]

---

[1]Now at CERN.
[2]Permanent address: Institut für Physik, Universität Dortmund, Fed. Rep. of Germany.
[3]Permanent address: DESY, Hamburg, Fed. Rep. of Germany.
[4]Now at Lecroy, Geneva.
[5]On leave of absence from University of Washington, Seattle, WA 98195.
[6]Now at FSU.
[7]Now at INFN Milano.
[8]Permanent address: LBL, California, USA.
[9]Supported by CAICYT, Spain.
[10]Supported by the Danish Natural Science Research Council.
[11]Supported by the UK Science and Engineering Research Council.
[12]Supported by the US Department of Energy, contract DE-AC02-76ER00881.
[13]Supported by the US Department of Energy, contract DE-FG05-87ER40319.
[14]Supported by the NSF, contract PHY-8451274.
[15]Supported by the US Department of Energy, contract DE-FC0S-85ER250000.
[16]Supported by SLOAN fellowship, contract BR 2703.
[17]Supported by the Bundesministerium für Forschung und Technologie.

Abstract

The cross-section for $e^+e^- \rightarrow$ hadrons in the vicinity of the Z boson peak has been measured with the ALEPH detector at the CERN Large Electron Positron collider, LEP. Measurements of the Z mass, $M_Z = (91.174 \pm 0.070)$ GeV, the Z width $\Gamma_Z = (2.68 \pm 0.15)$ GeV, and of the peak hadronic cross-section, $\sigma_{had}^{peak} = (29.3 \pm 1.2)$nb, are presented. Within the constraints of the Standard Electroweak Model, the number of light neutrino species is found to be $N_\nu = 3.27 \pm 0.30$. This result rules out the possibility of a fourth type of light neutrino at 98% C.L.

1 Introduction

The Z boson was discovered in 1983 at the $p\bar{p}$ collider at CERN [1], [2]. Detailed studies of its properties can now be performed in e^+e^- collisions at LEP. In the Standard Electroweak Model [3], the Z boson is expected to decay with comparable probability into all species of fermions that are kinematically allowed. The decay rate of the Z into light, neutral, penetrating particles such as neutrinos, that would otherwise escape detection, can be measured through an increase in the total width Γ_Z. Detection of additional neutrino species would put in evidence additional fermion families, even if the masses of their charged partners are inaccessible at presently available energies. One additional species of neutrino would result in an increase of 6.6% in Γ_Z. Furthermore the peak cross-section to any detectable final state f is very sensitive to this change and would decrease by 13% for one more neutrino species. This cross-section can be expressed in terms of Γ_Z and of the partial widths, Γ_{ee}, Γ_ν, Γ_f, of the Z into e^+e^-, neutrinos, and the final state f as:

$$\sigma_f^{peak} = \frac{12\pi}{M_Z^2}\frac{\Gamma_{ee}\Gamma_f}{\Gamma_Z^2}(1-\delta_{rad}) \equiv \sigma_f^0(1-\delta_{rad}), \tag{1}$$

with

$$\Gamma_Z = N_\nu\Gamma_\nu + 3\Gamma_{ee} + \Gamma_{had}, \tag{2}$$

where N_ν is the number of light neutrino species. In the particular case where f comprised mostly hadronic final states, uncertainties in the overall scale of partial widths, such as those related to the lack of knowledge of the top quark mass and more generally to electroweak radiative effects, as well as uncertainties in the ratio of hadronic to leptonic partial widths, largely cancel in this formula. The QED initial state radiative correction, δ_{rad}, is quite large, but has been calculated to an accuracy believed to be better than 0.5% by several authors [4].

Cross-sections are measured by taking the ratio of the number of selected Z decays, hereafter referred to as hadronic events, to the number of small angle e^+e^- events from the well calculable Bhabha scattering process, hereafter referred to as luminosity events.

2 Description of the ALEPH detector

The data presented here have been collected with the ALEPH detector during the first three weeks of running at LEP, from 20 September to 9 October 1989. Guided by earlier measurements of the Z mass by the CDF [5] and MarkII [6] collaborations, data were collected mainly at the Z peak and in the near vicinity of it. Integrated luminosities of 64 nb^{-1} at the peak and 88 nb^{-1} on the sides of the peak were recorded.

A detailed description of the ALEPH detector is in preparation [7]. The principal components relevant for this measurement are:

- The Inner Tracking Chamber, ITC, an 8-layer cylindrical drift chamber with sense wires parallel to the beam axis from 13cm to 29cm in radius. Tracks with

polar angles from 14° to 166° traverse all 8 layers.

- The large cylindrical Time Projection Chamber, TPC, extending from an inner radius of 31 cm to an outer radius of 180 cm over a length of 4.4 m. Up to 21 space coordinates are recorded for tracks with polar angles from 47° to 133°. Requiring 4 coordinates, tracks are reconstructed down to 15°.
- The Electromagnetic Calorimeter, ECAL, a lead wire-chamber sandwich. The cathode readout is subdivided into a total of 73,728 projective towers. Each tower of about $1° \times 1°$ solid angle is read out in three stacks of 10, 23 and 12 layers (respectively 4 ,9 and 9 radiation lengths). The signals from the 45 wire planes of each of the 36 modules are also read out. The two endcaps cover polar angles from 11° to 40° and 140° to 169° and the barrel covers polar angles from 40° to 140°.
- The superconducting, solenoidal coil, providing a magnetic field of 1.5 T.
- The Hadron Calorimeter, HCAL, comprised of 23 layers of streamer tubes interleaved in the iron of the magnet return yoke, read out by a total of 4608 projective towers. Signals from each of the tubes are also read out. The modules are rotated in azimuth by $\sim 2°$ with respect to the electromagnetic calorimeter so that inactive zones do not align in the two calorimeters. The two endcaps and the barrel of the hadron calorimeter cover polar angles down to 6°.
- The Small Angle Tracking chamber, SATR, with 9 planes of drift tubes, covering angles from 40 to 90 mrads, for precise measurement of small angle electron tracks.
- The Luminosity calorimeter, LCAL, similar in its construction and read-out to ECAL, extending from 50 to 180 mrads, providing energy and position measurement of the showers produced by luminosity events.

Hadronic events were triggered by two independent first level triggers: i) an ECAL-based trigger, requiring a total energy of 6 GeV deposited in the ECAL barrel or 3 GeV in either of the ECAL endcaps or 1 GeV in both in coincidence; ii) an ITC-HCAL coincidence, for penetrating charged particles, requiring 6 ITC wire planes and 4 to 8 planes of HCAL tubes in the same azimuthal region.

Luminosity events were also triggered in two ways: i) a coincidence of 15 GeV deposited in LCAL on one side with 10 GeV deposited on the other side, without requiring azimuthal correlation; ii) a single arm requirement of 32 GeV deposited in either side of LCAL. In addition, prescaled single arm triggers with 10 and 15 GeV thresholds were recorded to provide an estimate of the beam related background.

All types of events were processed simultaneously through the same trigger system (with the same dead-time), through the same data acquisition and reconstruction programs. In order to ensure that the events were counted during the same live-time, the list of enabled triggers and the status of each of the relevant subdetectors was recorded with each event. Events were accepted only when both ECAL and LCAL were running and when both ECAL and LCAL triggers were enabled. A possible

bias could come from the few data acquisition failures that occurred during the run. A careful investigation of all the events before, during, and after each failure revealed a possible but small loss of 0.4% of the hadronic events. This check could be done for the events that were mishandled because their trigger pattern was always recorded and the trigger patterns of hadronic and luminosity events are unique enough to allow an estimate of the losses in each category.

3 Event selection

To provide a check, two independent event selections were used. The first one selected hadronic Z decays only, and was based on TPC tracks. The second one selected decays of the Z into hadrons as well as τ pairs, and was based on calorimetric energy. The event samples overlapped to the extent of 95%. The efficiencies of both methods were very close to unity and systematic uncertainties in these efficiencies were less than 1%. Altogether 3112 events were retained in the track selection and 3320 events in the calorimetric selection.

3.1 Selection with TPC tracks

Hadronic Z decays (a typical event is shown in figure 1) were selected on the basis of charged tracks only, requiring at least 5 charged tracks. The energy sum of all charged tracks was required to be at least 10% of the centre-of-mass energy. Tracks were required to have a polar angle larger than 18.2°, to be reconstructed from at least 4 TPC coordinates, and to originate from a 2 cm radius 20 cm long cylinder around the nominal beam position. The performance of the TPC was in remarkable agreement with expectations. In order to estimate the acceptance, a complete simulation of the $e^+e^- \rightarrow$ *hadrons* process was performed, including initial state radiation effects and hadronization. The properties that are relevant for acceptance calculation, total charged-particle energy, track multiplicity, sphericity distribution and polar angle distribution, are in good agreement with the simulation, as shown in figure 2. The efficiency of this selection method is 0.975 ± 0.006, on the peak; the error corresponds to assigning a conservative 20% energy scale uncertainty near the cut. Uncertainties in hadronization models were reduced to a very small level by using the measured sphericity distribution for the acceptance calculation. Due to initial state radiation, this efficiency varies slightly on the side of the Z peak by up to -0.003.

Contamination of the sample of hadronic events by τ pairs from Z decays was estimated to be (5.1 ± 1.5) events, and in fact three events compatible with that hypothesis were found in the sample. Contamination by beam-gas interactions was estimated from the number of events found passing the selection cuts except for the longitudinal vertex position: about one event is expected. Finally the background from $e^+e^- \rightarrow e^+e^-$+hadrons ("two photon" events) was calculated to be about 15 pb, representing a contamination of 0.5×10^{-3} to the peak cross-section.

3.2 Selection using the calorimeters

The aim of this method was to select hadronic and τ events. The basic requirement was that the total calorimetric energy be above 20 GeV, as well as either $\geq$ 6 GeV in the ECAL barrel or at least 1.5 GeV in each ECAL endcap. These requirements reduce both two-photon events and muon-pair events to a negligible level. Large-angle e^+e^- events were rejected on the basis of their characteristic tight energy clusters in the electromagnetic calorimeter. For the few events with no tracks at all, cuts were applied to eliminate cosmic rays: a timing cut and a cut on the minimal number (2) of clusters above 3 GeV in ECAL. On the basis of Monte-Carlo simulation as well as the scanning of events the resulting selection efficiency is 0.994±0.005 for hadronic events and 0.60±0.05 for τ events, giving a combined $\sigma_{had} + \sigma_\tau$ efficiency of 0.974±0.006. Contamination by events other than hadronic or τ was estimated to be less than 0.4%.

The two event samples were compared event by event. Differences were well understood given the different characteristics of the two selections.

3.3 Trigger efficiency

The trigger efficiency was measured by counting events where one or both of the ECAL and ITC-HCAL triggers occurred; it was found to be 100% for the ECAL trigger and 87% for the ITC-HCAL trigger, giving an overall efficiency of 100%.

4 Determination of the Luminosity

Luminosity events were selected on the basis of the energy deposited in the LCAL towers. Neighboring towers containing more than 50 MeV were joined into clusters, giving energy and position of the shower. Events were required to have a shower reconstructed on each side of LCAL.

In order to minimize the dependence of the acceptance upon precise knowledge of the beam parameters, an asymmetric selection was performed: on one side (e.g., the e^+ side), showers were required to have more than half of their energy deposited in a fiducial volume (figure 3) excluding the towers situated at the edge of the detector; the total energy deposit on that side was also required to be larger than 55% of the beam energy; on the other side (e^-side), only a total energy deposition of more than 44% of beam energy was required. The respective roles of the e^+ and e^- sides were interchanged in every other event. Finally, the difference in azimuth , $\Delta\phi$, between the e^+ and the e^- was required to be larger than 170°

The accepted cross-section was calculated using a first order event generator [8] with a full simulation of the detector. The value obtained for the cross-section for Bhabha scattering into the region within these cuts was found to be ($31.12\pm0.45_{exp}$ $\pm$ 0.31_{th})nb, at a centre-of-mass energy of 91.0 GeV and for a Z mass of 91.0 GeV. The first error represents the effect of uncertainties in the simulation, calibration, and positioning of the apparatus; the second one represents the possible error due

transverse and longitudinal shower profile	$\pm$ 0.005
energy scale	$\pm$0.002
energy resolution and cell-to-cell calibration	$\pm$0.007
external alignment and beam parameters	$\pm$0.002
internal alignment and inner radius	$\pm$0.010
description of material	$\pm$0.005
higher order radiative effects	$\pm$0.01
total uncertainty:	$\pm$ 0.02

Table 1: Summary of systematic errors in the luminosity measurement

to neglecting higher order radiative effects, and the uncertainty in the photon vacuum polarization[9]. Properties of the luminosity events are shown in figure 4, and compared with the simulation. The optimum energy resolution has not yet been obtained, but the acceptance is quite insensitive to this. Other properties are in good agreement with expectations. The displacements of the beam were measured using luminosity events themselves and corrected for.

The beam-related background contamination was estimated from single arm, prescaled triggers. These triggers were combined into artificial double arm events. The number of such combinations passing the selection cuts was normalized to the number of real coincidences with $\Delta\phi < 90°$. This background subtraction was performed for each run and was of the order of 1% or smaller.

The contamination by physics sources such as $e^+e^- \to \gamma\gamma$ or $e^+e^- \to e^+e^- f\bar{f}$ has been estimated to be less than 2×10^{-3}. The interference of the Z exchange diagram with the purely QED contribution has been taken into account when determining the resonance parameters.

The trigger efficiency was measured for each data taking period by comparing the number of events passing the selection criteria that set the single arm trigger, the coincidence trigger, or both. Inefficiencies in the trigger were traced down to faulty electronic channels. Efficiencies vary with the run, ranging from 0.98 to 1.00 with an average value of 0.997 ± 0.002.

A summary of the luminosity systematic errors is given in table 1. A relatively small normalization error was possible mainly as a result of the excellent spatial resolution of the calorimeter ($\sim 300\mu$m for electrons near the tower boundaries), the good background conditions delivered by the machine, the availability of a redundant set of triggers and progress in the theoretical calculations [10]. The relative normalization uncertainty of cross-section measurements at different energies comes mostly from differences in background conditions and trigger efficiency. These uncertainties were taken into account in the statistical error.

Energy (GeV)	Selection from TPC tracks N_{had}	N_{Lumi}	σ_{had} (nb)	Selection by calorimeters $N_{had}+N_\tau$	N_{Lumi}	$\sigma_{had}+\sigma_\tau$ (nb)
89.263	120	443	9.00 ± 0.92	134	450	9.89 ± 0.97
90.265	406	715	18.43 ± 1.14	445	736	19.62 ± 1.17
91.020	656	668	31.29 ± 1.72	678	669	32.28 ± 1.76
91.266	1156	1295	28.16 ± 1.14	1243	1309	29.96 ± 1.19
92.260	258	377	21.11 ± 1.72	268	374	22.10 ± 1.78
92.519	125	247	15.52 ± 1.71	142	260	16.75 ± 1.76
93.264	391	883	13.36 ± 0.82	410	889	13.92± 0.84

Table 2: Event numbers and cross-section as a function of centre-of-mass energy. The overall systematic error of ±2% in the cross-sections is not included.

5 Determination of the Z resonance parameters

The number of Z events, of luminosity events, together with the cross-sections are given in table 2 for the two event selection methods.

Two different fits were performed to the data. In the first fit, the basic parameters of the Z resonance, its mass M_Z, width Γ_Z ,and QED corrected peak cross-section $\sigma_f^0 \equiv \frac{12\pi}{M_Z^2}\frac{\Gamma_{ee}\Gamma_f}{\Gamma_Z^2}$ are extracted with little model dependence. In the second fit, the constraints from the Standard Model are applied to determine M_Z and N_ν.

The three parameter fit was performed using computer programs by Burgers [11] and Borelli et al. [12], folding a Breit-Wigner resonance (with s-dependent width) with the second order exponentiated initial state radiation spectrum. Results from fitting with the two programs were in good agreement with each other. These approximate programs agree adequately with complete Electroweak calculations [13] for centre-of-mass energies within ± 2.5 GeV of the peak. These fits yield the following values for the mass and width of the Z boson:

	Hadronic events	Hadronic $+\tau$ events	Combined
M_Z (GeV)	91.178±0.055	91.170 ± 0.054	91.174 ± 0.054
Γ_Z (GeV)	2.66 ± 0.16	2.70 ± 0.15	2.68 ± 0.15
σ^0(nb)	39.1 ± 1.6	40.9 ± 1.7	–
σ^{peak}(nb)	29.3 ± 1.2	30.5 ± 1.3	–

The data points and the result of the fit are shown in figure 5 for the track selected events.

The error in M_Z does not yet include the uncertainty in the mean e^+e^- collision energy. This error was determined by the LEP division [14] on the basis of measurements of uncertainties in the magnetic field integrals and in the orbit positions to be 5×10^{-4} or 45 MeV. Including this uncertainty, we find:

Γ_{ee}(MeV)	83.5	$\pm$ 0.5
Γ_{ν}(MeV)	166.5	$\pm$ 1.0
Γ_{had}(MeV)	1737.	$\pm$ 22.

Table 3: Standard Model partial widths of the Z in MeV for the measured value of M_Z; $\alpha_s = 0.12 \pm 0.02$ and $sin^2\vartheta_w = 0.230 \pm 0.006$ have been used as input.

$$M_Z = (91.174 \pm 0.055_{exp} \pm 0.045_{LEP})\text{GeV} \tag{3}$$

The value agrees with the two previous best measurements [5] and [6], but the uncertainty is smaller by a factor of 2.

M_Z is effectively uncorrelated with the other two parameters. The correlation between Γ_Z and σ^0 for the track selected data sample is shown in figure 6.

In the Standard Model, Γ_{ee}, Γ_{had} and Γ_{ν} are calculable with a small uncertainty of about $\pm 1\%$ due to: i) Electroweak radiative effects involving unknown particles, such as the top quark; ii) the value of the strong coupling constant α_s. The Standard Model predictions for the partial widths are given in table 3. The Standard Model predictions for σ^0 and Γ_Z assuming 2,3, and 4 species of light neutrinos are shown in figure 6. The value $N_{\nu} = 3$ is preferred. More precise information on N_{ν} is contained in the peak cross-section σ^0.

If the partial widths are taken from Standard Model predictions, a two parameter fit can be performed, leaving M_Z and N_{ν} as only free parameters. This fit, performed with the programs of ref. [12] and [15] on the two data samples, leaves the value of M_Z unchanged. The result for N_{ν} is:

$$N_{\nu} = 3.27 \pm 0.24_{stat} \pm 0.16_{sys} \pm 0.05_{th}, \tag{4}$$

where the errors coming from statistics, experimental systematics and theoretical uncertainty are shown separately. Theoretical uncertainties due to Electroweak radiative effects consist mostly in a change of the overall scale of the partial widths, and largely cancel in σ^0. The uncertainty in Γ_{had}, related to the QCD correction, cancels in part in σ^0; the resulting uncertainty $\frac{\Delta\,\sigma^0}{\sigma^0} = 0.4\frac{\Delta\,\Gamma_{had}}{\Gamma_Z} = 0.003$ is much smaller than the effect produced by a single neutrino family, $\frac{\Delta\,\sigma^0}{\sigma^0} = -0.13$. Combining these errors in quadrature one finds:

$$N_{\nu} = 3.27 \pm 0.30. \tag{5}$$

The hypothesis $N_{\nu} = 4$ is ruled out at 98% confidence level. This measurement improves in a decisive way upon previous determinations of the number of neutrino species from the UA1 [16] and UA2 [17] experiments, from PEP [18] and PETRA [19], from cosmological [20] or astrophysical [21] arguments, as well as from a similar determination at the Z peak [22].

The demonstration that there is a third neutrino confirms that the τ neutrino is distinct from the e and μ neutrinos. The absence of a fourth light neutrino indicates

that the quark-lepton families are closed with the three which are already known, except for the possibility that higher order families have neutrinos with masses in excess of $\sim$ 30GeV.

6 Acknowledgements

We would like to express our gratitude and admiration to our colleagues of the LEP division for the timely and beautiful operation of the machine. We thank the Technical Coordinator, Pierre Lazeyras, and the technical staff of the ALEPH collaboration for their excellent work. We would like to dedicate this paper to the memory of those who died during LEP construction. Those of us from non-member countries thank CERN for its hospitality.

References

[1] G. Arnison et al.,(UA1 collab.), Phys. Lett. 126B,(1983) p. 398.

[2] P. Bagnaia et al.,(UA2 collab.), Phys. Lett. 129B (1983) p. 130.

[3] S.L. Glashow, Nucl. Phys., 22 (1961) p. 579;
S. Weinberg, Phys. Rev. Lett., 19 (1967) p. 1264;
A. Salam, Elementary Particle Theory, Ed. N.Svartholm, Stockholm, "Almquist and Wiksell" (1968), p. 367.

[4] R.N.Cahn, Phys. Rev. D36 (1987) p. 2666;
O.Nicrosini, L.Trentadue, Phys. Lett. B196 (1987) p. 551;
F.A.Berends, G.Burgers, W.Hollik, W.L.van Neerven, Phys. Lett. B203 (1988) p. 177;
G. Burgers, in 'Polarization at LEP', CERN 88-06 (1988);
D.Bardin et.al. Z-Line-Shape group, CERN-TH-5468 (1989);
D.C. Kennedy et al., Nucl. Phys. B321 (1989) p. 83.

[5] F. Abe et al., Phys. Rev. Lett. 63 (1989) 720.

[6] G. S. Abrams et al., Phys. Rev. Lett. 63 (1989) 724.

[7] "ALEPH - a Detector for electron-positron Annihilation at LEP", to be published in Nucl. Instr. Meth.

[8] F.A. Berends and R. Kleiss, Nucl.Phys. B228(1983)737; M.Böhm, A. Denner and W. Hollik, Nucl.Phys. B304(1988)687;
F.A. Berends, R. Kleiss and W. Hollik, Nucl.Phys. B304(1988)712.

[9] H.Burkhardt, F.Jegerlehner, G.Penso and C.Verzegnassi, Z.Phys.C43 (1989) p. 497.

[10] D. Y. Bardin et al., Monte Carlo working group, LEP Physics Workshop, CERN Yellow report to appear.

[11] Computer program ZAPP, courtesy of G. Burgers.

[12] A.Borelli, M.Consoli, L.Maiani, R.Sisto, CERN-TH.5441 (1989).

[13] D.Bardin et.al. Z-Line-Shape group, CERN-TH-5468 (1989).
Computer program ZHADRO, courtesy of G. Burgers.

[14] S. Myers, private communication and LEP note to appear.

[15] Computer program ZAPPH, courtesy of G. Burgers.

[16] C. Albajar et al. (UA1 Collab.), Phys. Lett. B185 (1987) p. 241.
C. Albajar et al. (UA1 Collab.), Phys. Lett. B198 (1987) p. 271.

[17] R. Ansari et al. (UA2 Collab.), Phys. Lett. B186 (1987) p. 440.

[18] W. T. Ford et al. (MAC Collab.), Phys. Rev. D19 (1986) p. 3472.
C. Hearty et al. (ASP Collab.), Phys. Rev. Lett. 58 (1987) p. 1711.

[19] H. J. Behrend et al. (CELLO Collab.), Phys. Lett. B215 (1988) p. 186.

[20] G. Steigman, K. A. Olive, D. N. Schramm and M. S. Turner, Phys. Lett. B176 (1986) p. 33.
J. Ellis, K. Enqvist, D. V. Nanopoulos and S. Sarkar, Phys. Lett. B167 (1986) p. 457.

[21] J. Ellis and K. A. Olive, Phys. Lett. B193 (1987) p. 525.
R. Schaeffer, Y. Declais and S. Jullian, Nature 330 (1987) p. 142.
L. M. Krauss, Nature 329 (1987) p. 689.

[22] J. M. Dorfan, (MarkII Collab.), International Europhysics Conference on High Energy Physics (Madrid,Spain) 7-14 Sep. 1989.

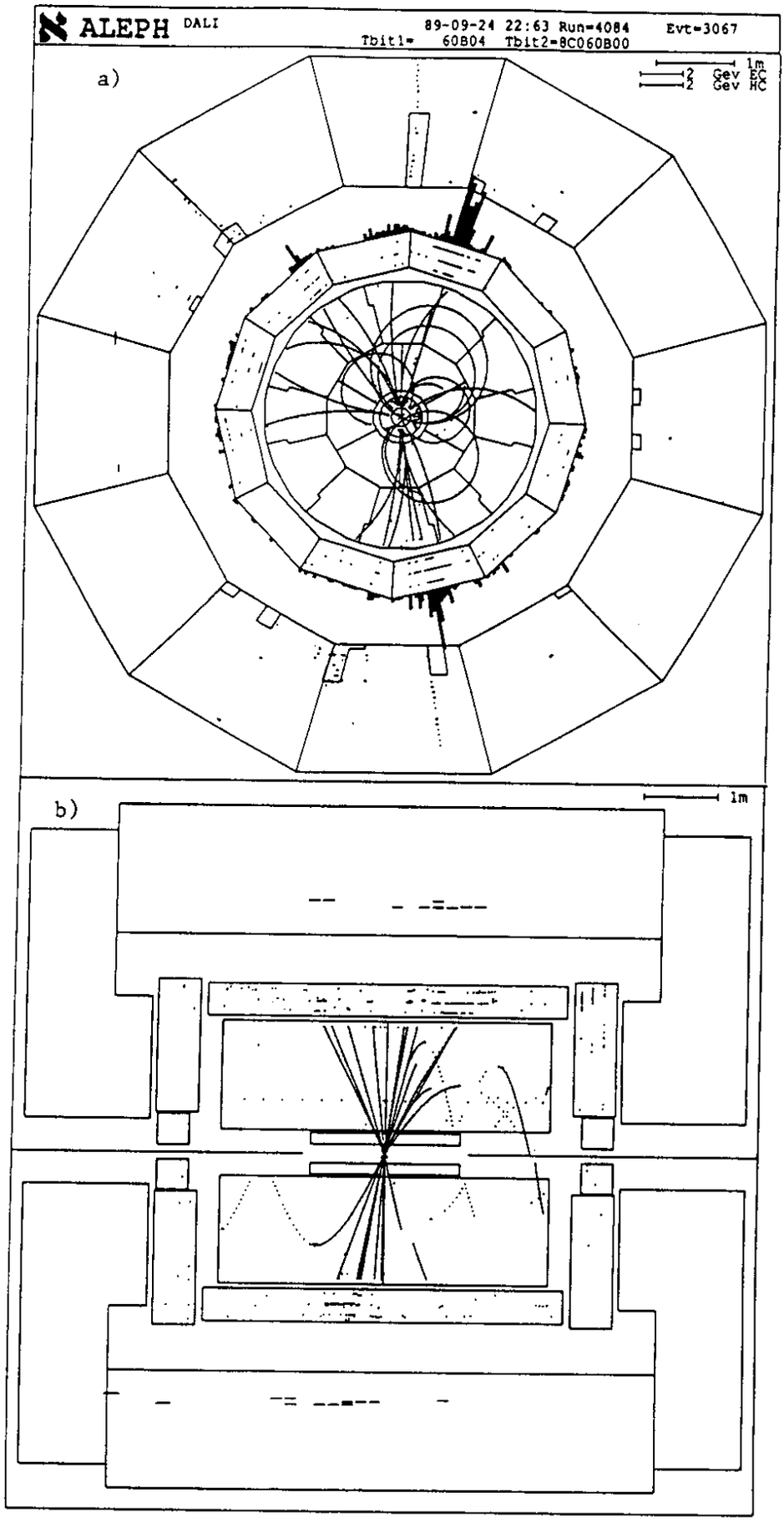

Figure 1: A hadronic Z decay in the ALEPH detector: a)x-y view; b) r-z view.

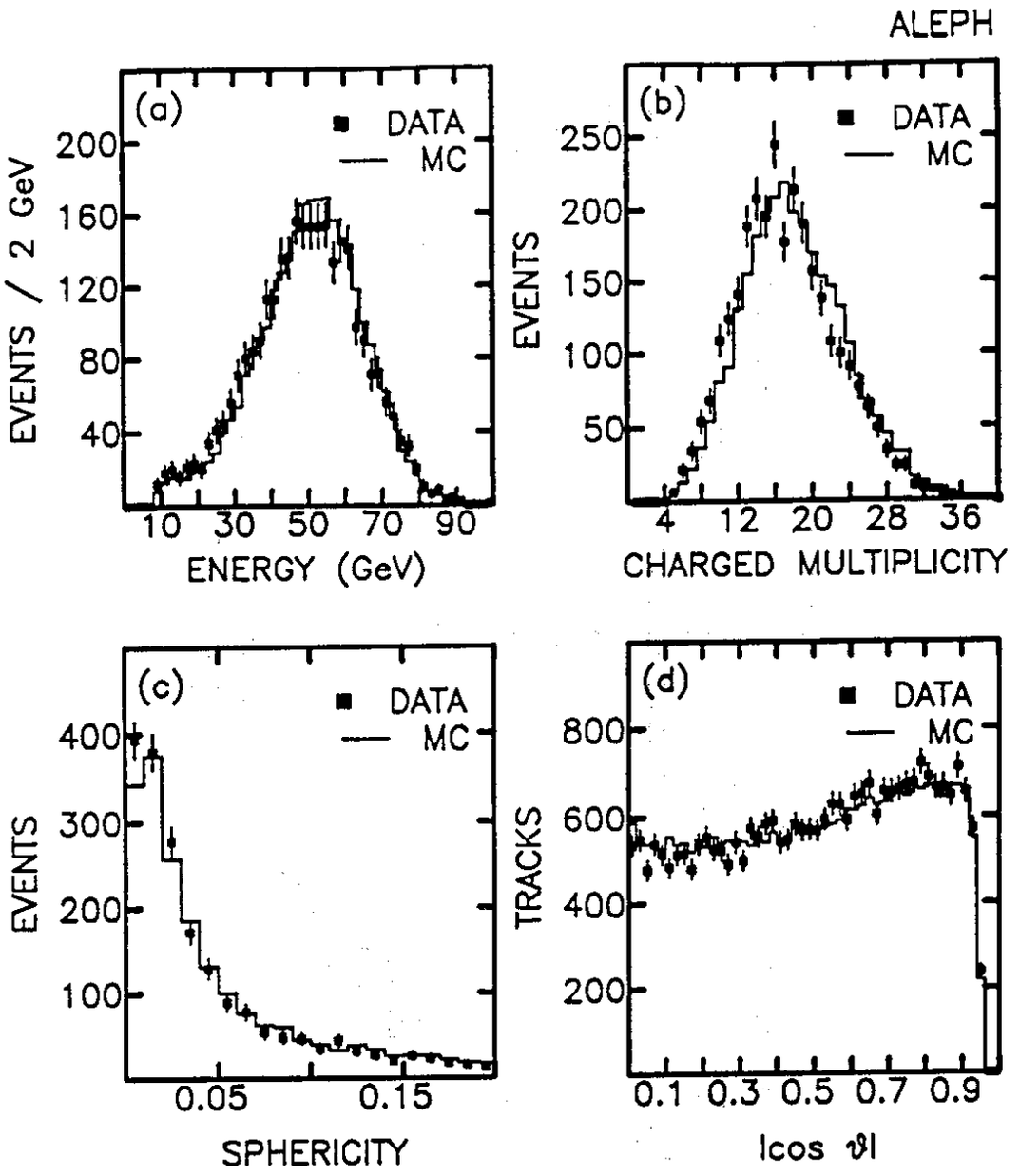

Figure 2: Properties of charged tracks in hadronic events and comparison with simulations. In each plot, the solid points represent data and the lines represent the simulation normalized to the data: a) distribution of the charged-track energy sum per event; b) charged-track multiplicity distribution; c) sphericity distribution for events where the sphericity axis had a polar angle such that $|cos\theta_{sph}| < 0.8$; and d) polar angle distribution for charged tracks.

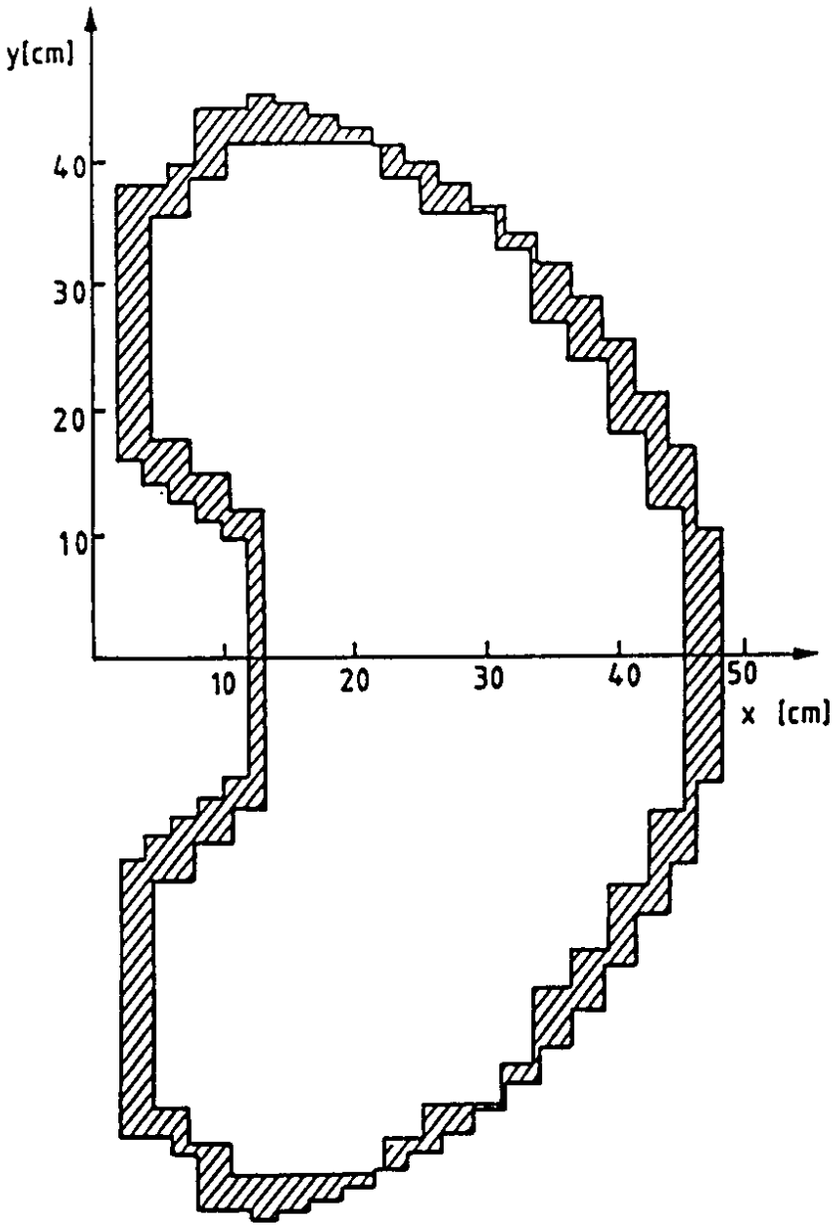

Figure 3: End view of the Luminosity Calorimeter, showing the tower limits; the shaded area represent the towers excluded from the fiducial area.

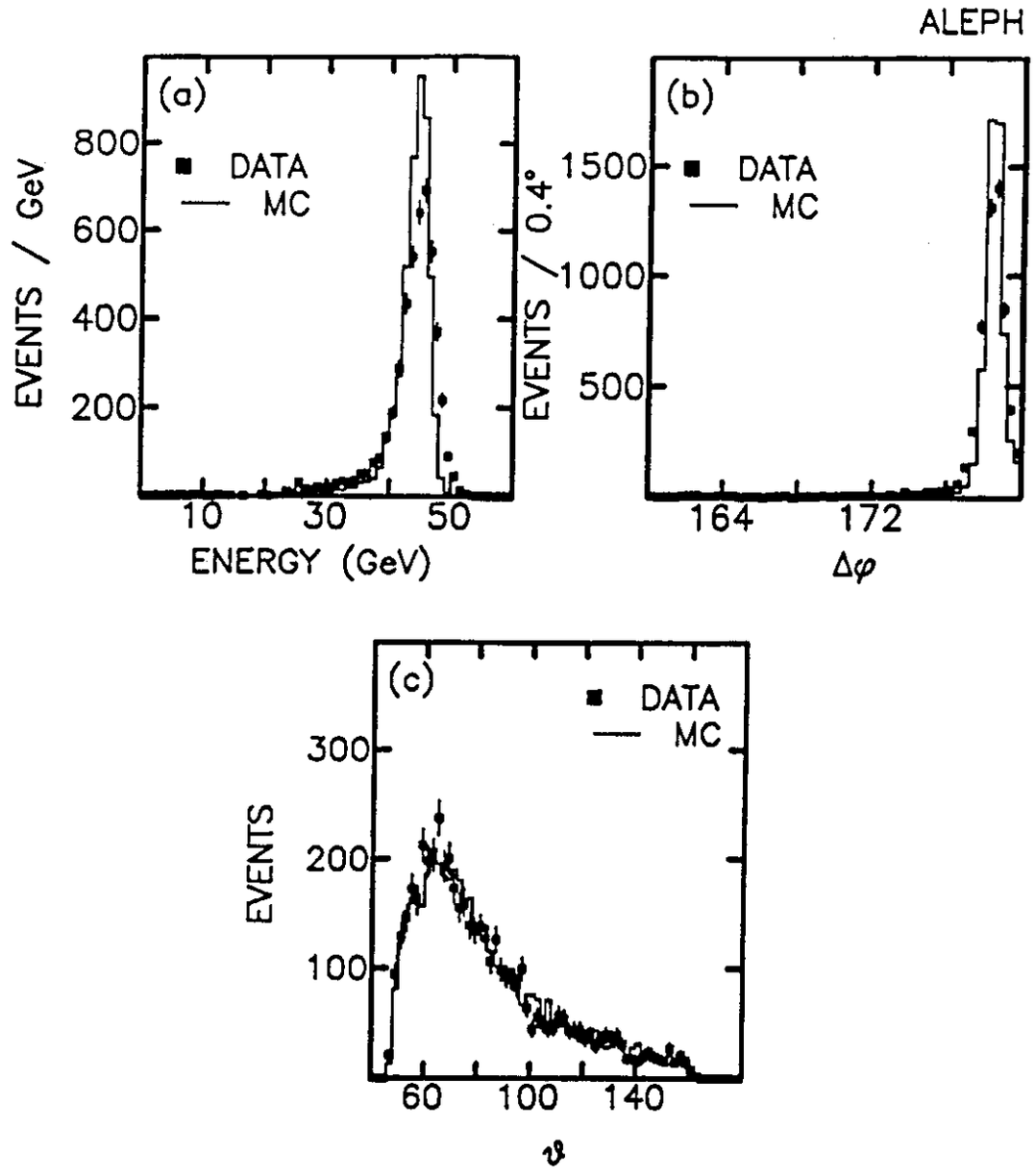

Figure 4: Properties of luminosity events passing selection criteria and comparison with simulations. In each plot, the solid points represent data and the lines represent the simulation normalized to the data: a) shower energy distribution for events passing the tight fiducial cut; b) azimuthal separation $\Delta\phi$ of the two opposite clusters; c) polar angle distribution.

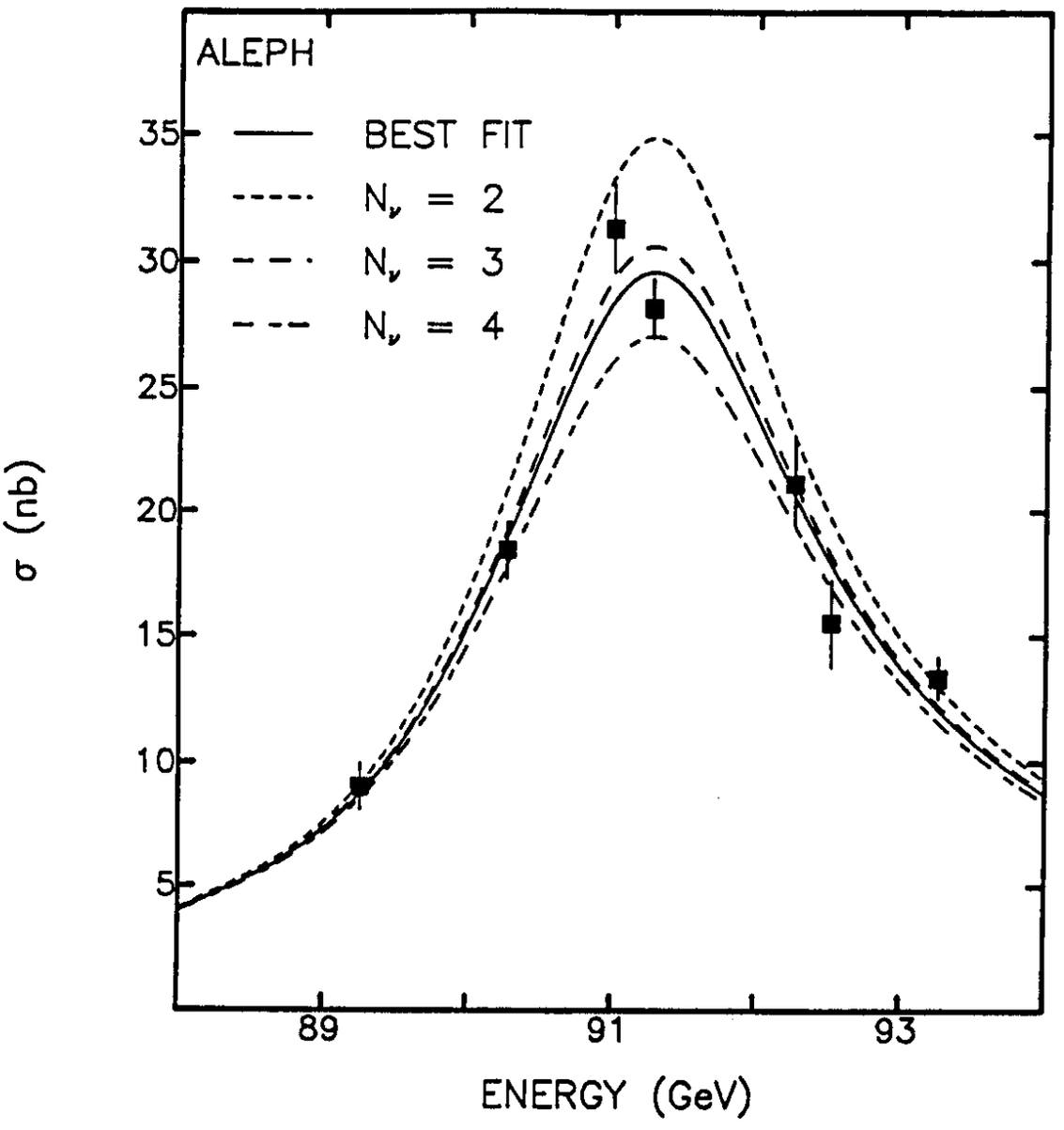

Figure 5: The cross-section for $e^+e^- \rightarrow$ hadrons as a function of centre-of-mass energy and result of the three parameter fit.

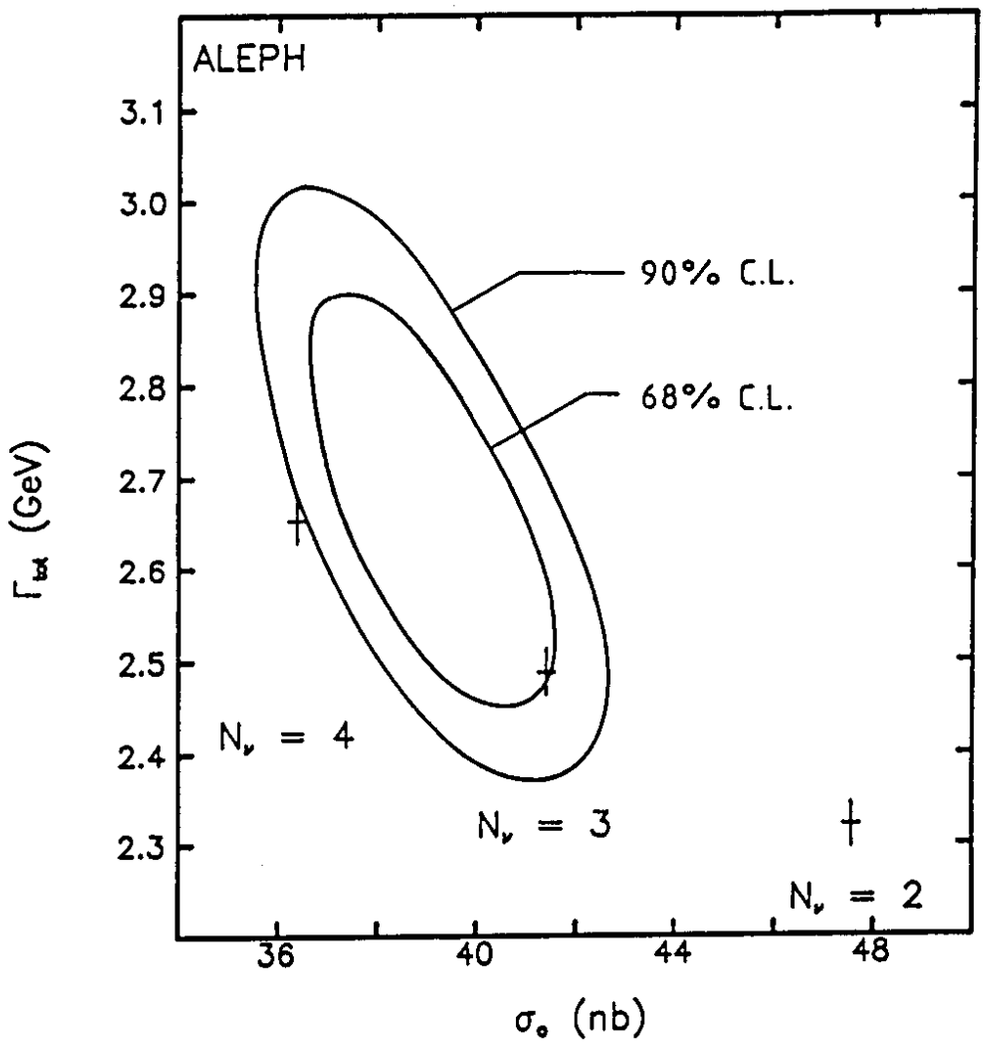

Figure 6: The total width versus the peak hadronic cross-section, with 68% and 90% C.L. experimental contours. The Standard Model prediction for 2,3 or 4 species of neutrinos is also shown, with its theoretical error.